loop, which starts at the freestream toward the low-velocity side, closes again toward the high-velocity side and contains two regions of countergradient transport (i.e., where $\partial\overline{U}/\partial n$ and $-\overline{uv}$ are of opposite signs). In the near wake, where the mean shear has regions of opposite signs, the loop extends over all four quadrants, but, farther downstream, it shrinks within the same quadrant as the freestream points. Despite its apparent local failure, gradient transport seems appropriate for a global description of the wake, if the loop is approximated by a straight line passing through the origin. The slope of this line, corresponding to the average eddy viscosity in the wake, was considerably lower than that in the outer flow, although their difference decreased with streamwise distance (Fig. 4b). By contrast to the rectilinear flow, gradient transport failed locally as well as globally to describe the thin wake in the curved flow (Fig. 4c), where the mean line through the data loops could not be made to pass through the origin. This is not so much an effect of the wake, but a general limitation of this concept in curved flows.

References

[1]Tavoularis, S., and Karnik, U., "Further Experiments on the Evolution of Turbulent Stresses and Scales in Uniformly Sheared Turbulence," *Journal of Fluid Mechanics*, Vol. 20, 1989, pp. 457–478.

[2]Holloway, A. G. L., and Tavoularis, S., "The Effects of Curvature on Sheared Turbulence," *Journal of Fluid Mechanics*, Vol. 237, 1992, pp. 569–603.

[3]Blackwelder, R. F., and Chang, S. I., "Length Scales and Correlations in a LEBU Modifided Turbulent Boundary Layer," AIAA Paper 86-0287, 1986.

[4]Bonnet, J. P., Delville, J., and Lemay, J., "Study of LEBUs in Modified Turbulent Boundary Layer by Use of Passive Temperature Contamination," Proceedings of the Symposium on Turbulent Drag Reduction by Passive Means, Royal Aeronautical Society, 1987.

[5]Bandyopadhyay, P. R., and Watson, R. D., "Pressure Field due to Drag Reducing Outer Layer Devices in Turbulent Boundary Layers," *Experiments in Fluids*, Vol. 5, 1987, pp. 393–400.

Subsonic Boundary-Layer Tripping by Strip Blowing

J. A. Masad* and R. Abid†
High Technology Corporation, Hampton, Virginia 23666
and
A. S. Abdelnaser‡
Virginia Polytechnic Institute and State University, Blacksburg, Virginia 24061

THE achievement of earlier transition by artificial tripping of the boundary layer is often desired in wind-tunnel operations to simulate turbulent boundary-layer behavior at full-scale Reynolds numbers. The most common method for tripping the boundary layer is the use of roughness. The existence of roughness enhances the instability of the flow and accelerates the onset of transition and, consequently, the occurrence of turbulence. This approach to tripping the boundary layer with roughness elements becomes more difficult at higher speeds. A major difficulty associated with the use of roughness is that it can cause flow separation and can lead to global breakaway of the flow and vortex shedding, which prevent the formation of a "clean" attached turbulent boundary layer. For this reason, research into alternate techniques for tripping the boundary layer that may avoid the difficulties associated with the use of roughness is necessary.

Received Dec. 2, 1994; revision received Feb. 6, 1995; accepted for publication Feb. 7, 1995.

*Research Scientist, 28 Research Drive. Senior Member AIAA.

†Senior Research Scientist, 28 Research Drive. Member AIAA.

‡Visiting Assistant Professor, Department of Engineering Science and Mechanics. Member AIAA.

The occurrence of laminar separation on aerodynamic surfaces increases pressure drag and reduces lift, which results in a reduction in the efficiency of these surfaces. Separation can result from a localized adverse pressure gradient created by surface roughness,[1] or it can result from extended regions of adverse pressure gradient due to the curvature of the surface. In both cases, the flow may separate while it is still laminar. Masad and Malik[2] showed that at certain conditions the location of transition onset is further downstream of the location of the onset of separation. This phenomenon is particularly true at low unit Reynolds numbers, at increasing Mach numbers, or in the presence of a short roughness element. In situations in which laminar separation is about to occur, tripping the boundary layer so that it remains attached is preferable. Transition causes the point of separation to move downstream because in a turbulent boundary layer the accelerating influence of the external flow extends farther due to turbulent mixing. In turn, the dead area decreases considerably, which reduces the pressure drag. These phenomena are the second reason for studying alternative techniques for tripping the boundary layer. In this work, we study the effect of using strip blowing on the location of transition onset in subsonic flow over a flat plate. We use linear stability theory, coupled with the empirical e^N method, to predict the transition onset location.

We consider a two-dimensional subsonic flow over a flat plate in the presence of discrete blowing. As a result of the discrete blowing, both a viscous-inviscid interaction and an upstream influence exist, and we use the interacting boundary layer (IBL) theory to analyze the flowfield (see Davis[3]). Extensive details of the IBL formulation for two-dimensional subsonic flow are given by Nayfeh and Abu Khajeel (see Abu Khajeel[4]). In cases with suction or blowing, the velocity of the flow through the surface is denoted by v_w and is made nondimensional with respect to the freestream streamwise velocity U^*_∞. For suction, v_w is negative; for blowing, v_w is positive. The length of the suction or blowing strip is denoted by λ.

In stability analysis, small, unsteady two-dimensional disturbances are superimposed on the mean-flow quantities, which are computed with the IBL theory. Mack[5] showed that the most amplified waves in two-dimensional flow with a freestream Mach number M_∞ of less than approximately 0.8 are two-dimensional waves. Next, the total quantities are substituted into the Navier–Stokes (NS) equations, the equations for the basic state are subtracted out, the quasiparallel assumption is invoked, and the equations are linearized with respect to the disturbance quantities. The disturbance quantities are assumed to have the normal-mode form, so that a disturbance quantity $\hat{q}$ is

$$\hat{q} = \xi(y) \exp i(\alpha x - \omega t) + \text{complex conjugate} \tag{1}$$

The streamwise coordinate is x, t is the time, and α and ω are generally complex. In the stability analysis and the computations throughout this work, the reference length is $\delta^*_r = \sqrt{\nu^*_\infty x^*/U^*_\infty}$, the reference velocity is U^*_∞, the reference time is δ^*_r/U^*_∞, the reference temperature is the freestream temperature T^*_∞, the reference viscosity is the freestream dynamic viscosity μ^*_∞, and the pressure is made nondimensional with respect to $\rho^*_\infty U^{*2}_\infty$ (where ρ^*_∞ is the freestream density). The viscosity varies with temperature in accordance with Sutherland's formula; the specific heat at constant pressure C^*_p is constant, and the Prandtl number Pr is constant and equal to 0.72. For the spatial stability of the two-dimensional flow considered in this work, ω is real, and α is complex, where the real part α_r is the streamwise wave number and the negative of the imaginary part $-\alpha_i$ is the spatial growth rate. The frequency ω is related to the dimensional circular frequency ω^* through $\omega = \omega^*\delta^*_r/U^*_\infty$, which leads (with the definition of δ^*_r) to

$$\omega = FR \tag{2}$$

where

$$F = \frac{\omega^* \nu^*_\infty}{U^{*2}_\infty} \tag{3}$$

and

$$R = U^*_\infty \delta^*_r/\nu^*_\infty = \sqrt{xRe} = \sqrt{Re_x} \tag{4}$$

Because ω^* is fixed for a certain physical wave as it is convected downstream, F is also fixed for the same wave.

The preceding normal-mode form separates the streamwise and temporal variations. The resulting equations and corresponding boundary conditions form an eigenvalue problem that can be solved numerically. For the results presented in this work, the computations were performed with an adaptive second-order-accurate finite difference scheme with deferred correction.[6]

By solving the linear instability eigenvalue problem, we obtain the disturbance wave growth rate as a function of location on the flat surface. The transition onset location is then empirically correlated with the location at which the integrated growth rate (N factor) of the disturbance wave reaches a certain value. This is an empirical transition onset criterion called the N-factor criterion (i.e., the criterion that utilizes the e^N method) proposed by Smith and Gamberoni[7] based on experimental data. (See also Jaffe et al.[8]) For flow over a flat plate, transition was found to occur when the N factor reached a value close to 9; we use this value throughout this work to correlate the location of transition onset. We denote the value of Re_x at which the N factor reaches a value of 9 by $(Re_x)_{N=9}$.

We present results on the effect of a mass-transfer (suction or blowing) strip on the predicted transition onset location for conditions that simulate single-frequency (controlled or forced) transition. Single-frequency transition is commonly used in wind-tunnel experiments in which a single-frequency monochromatic disturbance wave is introduced into the flowfield by a vibrating ribbon, for example. To compare the theoretically predicted transition onset location with that obtained from a single-frequency experiment, the location at which the N-factor value of a specific frequency disturbance reaches a value 9 can be determined theoretically and compared with the experimental transition onset location. The frequency that results in an N-factor value of 9 in the shortest distance from the leading edge is usually referred to as the most amplified frequency. For subsonic flow over an impermeable flat plate with a freestream Mach number $M_\infty = 0.8$, the most amplified frequency is $F = 10 \times 10^{-6}$. We considered a suction strip of length $\lambda = 0.2$ and uniform suction of $v_w = -5 \times 10^{-5}$ within the strip at $Re = 10^6$. The suction strip was placed at various locations, and the corresponding predicted transition onset locations at $F = 10 \times 10^{-6}$ were determined. The same calculations were performed for a blowing strip with $v_w = 5 \times 10^{-5}$. The results of both sets of calculations are presented in Fig. 1, in which we show variations of the predicted transition onset Reynolds number $(Re_x)_{N=9}$ with the Reynolds number $(Re_x)_C$, which is based on the distance from the leading edge of the flat plate to the center of the mass-transfer strip. The three vertical lines in Fig. 1 represent the locations of branch I, the maximum growth rate, and branch II of flow over an impermeable flat plate. The horizontal line is the predicted transition onset location of flow over an impermeable flat plate. Figure 1 clearly shows that the optimal stabilizing location of the suction strip is slightly downstream of branch I of flow over an impermeable flat plate. Furthermore, the most destablizing location of the blowing strip is also slightly downstream of branch I of flow over an impermeable flat plate.

Next, we present results that simulate wideband (natural) transition. To do so, a mass-transfer strip with a certain level of mass transfer and placed at a certain location is considered, and the lowest predicted transition onset Reynolds number over all frequencies is determined along with its most amplified frequency. Such calculations were performed for incompressible flow and with a strip of length $\lambda = 0.2$ at $Re = 10^6$. A high level of suction ($v_w = -5.6 \times 10^{-4}$) and three levels of blowing ($v_w = 0.5 \times 10^{-4}$, 1×10^{-4}, and 5×10^{-4} are considered. These levels of suction and blowing are high compared with those used in the calculations for Fig. 1. However, they are on the order of those used in laminar flow control. The mean flow calculations at such levels of suction and blowing are accurate because the IBL accounts for the viscous-inviscid interaction. The results of the calculations are shown in Fig. 2. If we compare Fig. 2 with Fig. 1, then we notice that the most stabilizing location of a suction strip (which was slightly downstream of branch I with single-frequency transition conditions) shifts downstream at wideband transition conditions. Actually, the most stabilizing location of a suction strip is downstream of the maximum growth rate point (the vertical dashed line in Fig. 2) of the most amplified frequency of incompressible flow over an impermeable flat plate (i.e., the maximum growth rate of $F = 26 \times 10^{-6}$). This determination of the optimal stabilizing location of a suction strip at wideband transition conditions agrees with the findings of Masad and Nayfeh.[9] On the other hand, the most destabilizing location of the blowing strip (also slightly downstream of branch I at single-frequency transition conditions) shifts upstream under wideband transition conditions. By increasing the blowing level within the strip, the most destabilizing location of the blowing strip moves further upstream of branch I of the most amplified frequency ($F = 26 \times 10^{-6}$) for incompressible flow over an impermeable flat plate. The destablizing effect of blowing and stabilizing effect of suction were noticed in low-speed laminar flow control experiments such as the experiments of Reynolds and Saric[10] and Saric and Reed.[11]

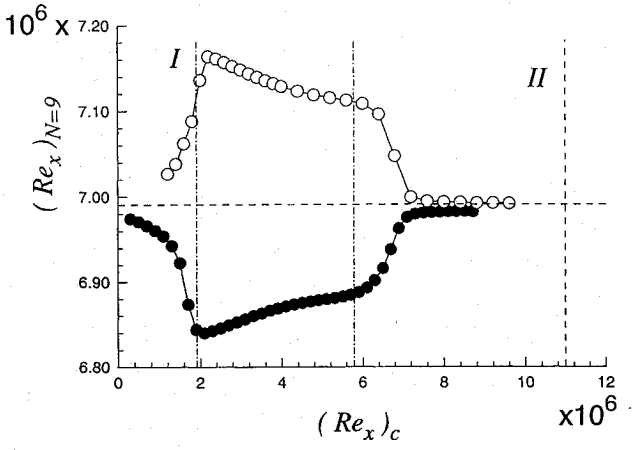

Fig. 1 Variation of predicted transition Reynolds number with Reynolds number based on location of mass-transfer strip for flow at M_∞ = 0.8, T^*_∞ = 300 K, $Re = 10^6$, $F = 10 \times 10^{-6}$, and $\lambda = 0.2$ with (○) $v_w = -5 \times 10^{-5}$ (suction) and (●) $v_w = 5 \times 10^{-5}$ (blowing).

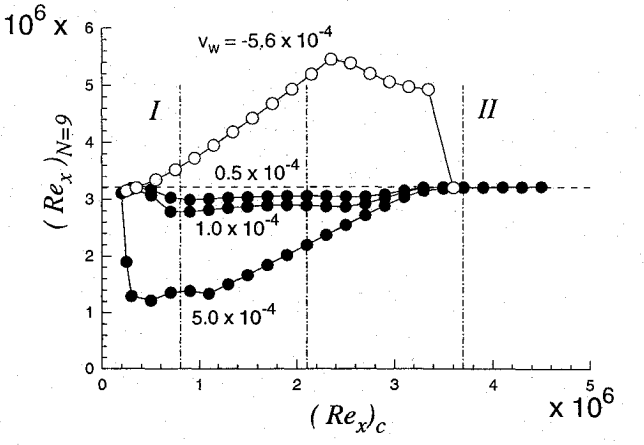

Fig. 2 Variation of predicted transition Reynolds number with Reynolds number based on location of mass-transfer strip for incompressible flow at $Re = 10^6$ and $\lambda = 0.2$.

In summary, the optimal destabilizing location of a blowing strip in subsonic flow for single-frequency (controlled or forced) transition conditions is slightly downstream of branch I of the considered single frequency. For wideband (natural) transition conditions, the optimal destabilizing location of a blowing strip is upstream of branch I of the most amplified frequency for flow over an impermeable flat plate. For wideband transition conditions, an increase in the blowing level within the strip moves the optimal destabilizing location upstream.

References

[1]Masad, J. A., and Iyer, V., "Transition Prediction and Control in Subsonic Flow over a Hump," *Physics of Fluids*, Vol. 6, No. 1, 1994, pp. 313–327.

[2]Masad, J. A., and Malik, M. R., "On the Link Between Flow Separation and Transition Onset," AIAA Paper 94-2370, 1994.
[3]Davis, R. T., "A Procedure for Solving the Compressible Interacting Boundary Layer Equations for Subsonic and Supersonic Flows," AIAA Paper 84-1614, 1984.
[4]Abu Khajeel, H. T., "Effect of Humps on the Stability of Boundary Layers over an Airfoil," M.S. Thesis, Virginia Polytechnic Inst. and State Univ., Blacksburg, VA, 1993.
[5]Mack, L. M., "Boundary-Layer Stability Theory," Jet Propulsion Lab., Document 900-277 (Rev. A), Pasadena, CA, 1969.
[6]Pereyra, V., "PASVA3: An Adaptive Finite-Difference Fortran Program for First-Order Nonlinear Ordinary Boundary-Value Problems," *Lecture Notes on Computer Science*, Vol. 76, 1976, p. 67.
[7]Smith, A. M. O., and Gamberoni, N., "Transition Pressure Gradient, and Stability Pressure Theory," Douglas Aircraft Co., Rept. ES 25388, El Segundo, CA, 1956.
[8]Jaffe, N. A., Okamura, T. T., and Smith, A. M. O., "Determination of Spatial Amplification Factors and Their Application to Predicting Transition," *AIAA Journal*, Vol. 8, No. 2, 1970, pp. 301–308.
[9]Masad, J. A., and Nayfeh, A. H., "Laminar Flow Control of Subsonic Boundary Layers by Suction and Heat-Transfer Strips," *Physics of Fluids A*, Vol. 4, No. 6, 1992, pp. 1259–1272.
[10]Reynolds, G. A., and Saric, W. S., "Experiments on the Stability of Flat-Plate Boundary Layer with Suction," *AIAA Journal*, Vol. 24, No. 2, 1986, pp. 202–207.
[11]Saric, W. S., and Reed, H. L., "Effect of Suction and Weak Mass Injection on Boundary-Layer Transition," *AIAA Journal*, Vol. 24, No. 3, 1986, pp. 383–389.

Actuator Placement with Failure Consideration for Static Shape Control of Truss Structures

Saburo Matunaga*
Tokyo Institute of Technology, Tokyo 152, Japan
and
Junjiro Onoda†
Institute of Space and Astronautical Science, Sagamihara 229, Japan

Introduction

ACTIVE control using actuators to obtain high accuracy of the static shape of large space structures is proposed. Unlike vibration control, high-control performance in static shape control is primarily determined by actuator location. A great deal of effort has been made in the last few years on techniques for solving for the optimal actuator placement or the integer optimization problem.[1,2] What seems to be lacking, however, is to evaluate the fault tolerance of the obtained actuator placement. In this Note, actuator failures are taken into consideration in the process of optimization.[3] In space applications actuator failure may occur, for example, at liftoff of the rocket, in the process of deployment and construction of the space structures and during operation of the actuators. Because it is so costly to repair or exchange a failed actuator in space, the actuators should be located so as to meet mission requirements even in the event of failure.

In this Note, actuator failure models are classified and their formulation is given. The optimization problem in this study is explained, and the results of computational simulations using a realistic example are discussed. The genetic algorithm (GA) method is used as the optimizer in these simulations.

Received Aug. 18, 1994; revision received Jan. 19, 1995; accepted for publication Jan. 20, 1995.

*Research Associate, Department of Mechano-Aerospace Engineering, Meguro-ku. Member AIAA.
†Professor, Research Division of Space Transportation, Yoshinodai. Member AIAA.

Optimal Shape Control Law

It is assumed that static distortion has occurred due to errors in the element length of truss structures e. When the system is assumed to be linear, the sensed distortion $\boldsymbol{u}$ is obtained as[4]

$$\boldsymbol{u} = \Psi \boldsymbol{e} + \boldsymbol{B}\theta = \psi + \boldsymbol{B}\theta \tag{1}$$

where ψ is the distortion caused by the length errors of the truss members, $\boldsymbol{\theta}$ is the vector of actuations of the actuators, and Ψ and $\boldsymbol{B}$ are the matrices which represent their effects. The quadratic distortion measure can be expressed by a proper weighting matrix $\boldsymbol{W}$ as follows:

$$u_{\text{rms}}^2 = \boldsymbol{u}^T \boldsymbol{W} \boldsymbol{u} \tag{2}$$

The actuators are controlled such that the quadratic measure is minimized based on the measured distortion, then the residual distortion and distortion measure after the optimal control become

$$\delta \equiv \boldsymbol{u}_{\text{opt}} = (\boldsymbol{I} - \boldsymbol{B}\boldsymbol{A}^{-1}\boldsymbol{B}^T\boldsymbol{W})\psi = \boldsymbol{G}\psi \tag{3}$$

$$\delta_{\text{rms}}^2 = \psi^T(\boldsymbol{W} - \boldsymbol{W}\boldsymbol{B}\boldsymbol{A}^{-1}\boldsymbol{B}^T\boldsymbol{W})\psi = \psi^T\boldsymbol{Q}\psi \tag{4}$$

where $\boldsymbol{A} = \boldsymbol{B}^T\boldsymbol{W}\boldsymbol{B}$. The effectiveness of the shape correction is measured by, e.g.,[4]

$$g^2 = E\left[\delta_{\text{rms}}^2\right]/E[\psi^T\boldsymbol{W}\psi] = \text{tr}[\boldsymbol{Q}\boldsymbol{C}_{\psi\psi}]/\text{tr}[\boldsymbol{W}\boldsymbol{C}_{\psi\psi}] \tag{5}$$

where $E[\,]$ denotes the expectation, tr[ ] refers to the trace of matrix[ ], and $\boldsymbol{C}_{\psi\psi}$ is the covariance matrix obtained from the covariance matrix of e.

Actuator Failure Models

Classification

Actuator failure models are considered in this section.[3] They may be divided into two main types as control system can identify the failed actuator A-1, and control system can not identify the failed actuator A-2. They can be further classified into the following three types, when an actuator is failed, the failed actuator fastens the member B-1, the failed actuator releases the member B-2, and the failed actuator actuator out of control B-3. Moreover, B-1 may be grouped into the following: the length of the failed active member is fixed to the initial length, in other words, it is regarded as a passive member B-1-1, and the length is fixed to the last length under control B-1-2, namely, it is regarded as the passive member whose length error is superimposed with the last actuated value of the actuator, where it is understood that the control effectiveness is not affected by the actuator's stiffness provided its stroke is long enough.[2] We can divide B-3 into two types: the actuated value of the failed actuator is correlated with the control value B-3-1, and the actuated value is not correlated with the control value B-3-2.

Formulation

In this Note, we concentrate on the simplest failure model: A-1 and B-1-1. The number of failed actuators is assumed to be only one, though it is easy to extend the analysis to several failed actuators. Similar to Haftka and Adelman,[1] this section develops a rigorous evaluation of the control measure, Eq. (5), due to removing one actuator. Removing the ith actuator can be simulated by performing the minimization of Eq. (2) under the constraint that $\theta_i = 0$. Employing Lagrange multipliers, we search for stationary points of ϕ_i where

$$\phi_i = \boldsymbol{u}^T\boldsymbol{W}\boldsymbol{u} - 2\lambda \boldsymbol{e}_{fi}^T\theta \tag{6}$$

where $\boldsymbol{e}_{fi}$ is a vector with unity in the ith row and zeros elsewhere, and $\boldsymbol{e}_{fi}^T\theta = \theta_i$. From stationary conditions, the distortion measure, Eq. (2), becomes

$$\delta_{\text{rms}}^{2(i)} = \psi^T\boldsymbol{Q}\psi + \lambda \boldsymbol{e}_{fi}^T\boldsymbol{S}\psi + \lambda^2 \boldsymbol{e}_{fi}^T\boldsymbol{U}\boldsymbol{e}_{fi} \tag{7}$$